

Chapter 2

Fundamentals of Experimental Visualization

Abstract An explanation is given on visualization techniques used in cold model experiments for refining processes agitated by gas injection. The topics include bubble generation methods, a typical experimental setup, choice of seeding particles, and image analyses. Various types of bubble generation methods have been proposed in order to meet requirement of researchers and engineers engaged in materials engineering. Most of them are briefly reviewed in this chapter. A previously used experimental setup is introduced for particle image velocimetry measurements of a flow in a bottom-blown bath. Scattering and tracking characteristics are explained for the choice of seeding particles. Finally, some algorithms for particle tracking velocimetry (PTV) are reviewed.

2.1 Generation Method of Bubble and Droplet

2.1.1 Generation Method of Bubble

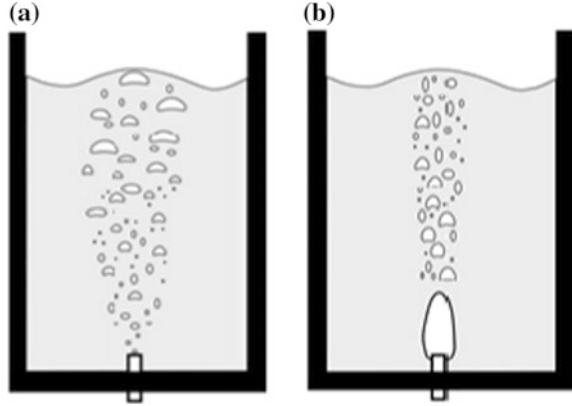
Many efforts have been devoted to generate bubbles of different diameters in materials engineering for the enhancement of process efficiency [1, 2]. In particular, generation of fine bubbles is one of the key technologies [3, 4]. Various kinds of methods therefore have been proposed on the basis of cold model experiments as listed below.

(1) Single-hole nozzle

Bubbles can readily be generated using a single-hole nozzle, as schematically shown in Fig. 2.1 [1, 5]. Gas is introduced into a liquid bath through the nozzle. There exist two types of bubble generation patterns: bubbling and jetting. The limit between the two types can be described by the following relation:

$$M = \frac{v_n}{c} = 1 \tag{2.1}$$

Fig. 2.1 Bubbling and jetting phenomena in a cylindrical bath agitated by centered bottom gas injection.
a Bubbling, **b** jetting



$$v_n = \frac{4Q_g}{\pi d_n^2} \quad (2.2)$$

where M is the Mach number ($-$), v_n is the gas velocity in the nozzle (m/s), c is the speed of sound of the gas (m/s), Q_g is the gas flow rate (m^3/s), and d_{ni} is the inner nozzle diameter (m). Bubbles are successively generated at the nozzle exit in the bubbling regime ($M < 1$), while a gas column is formed above the nozzle and its tip breaks up into many small bubbles in the jetting regime ($M \geq 1$).

In recent years, nano- and microbubbles attract much interest of researchers and engineers in mechanical, chemical, environmental, and materials engineering [3, 4]. The definitions of nano- and microbubbles are not clearly given. Roughly speaking, the diameter of nanobubble is smaller than several hundred nanometers and that of microbubble ranges from $10 \mu\text{m}$ to several hundred μm . Microbubbles can be generated, for example, using a needle-like single-hole nozzle.

Bubble formation in the bubbling regime depends strongly on the wettability of the nozzle, especially under low gas flow rate conditions [1]. The inner diameter, d_{ni} , affects the bubble size for a wetted nozzle, while the outer diameter, d_{no} , plays an essential role for a poorly wetted nozzle, as schematically shown in Fig. 2.2. That is, a smaller bubble can be generated using a wetted nozzle. The wettability can be quantitatively evaluated in terms of the equilibrium contact angle, θ , defined in Fig. 2.3. A solid body is wetted by a liquid for $0^\circ \leq \theta < 90^\circ$, while poorly wetted for $90^\circ \leq \theta \leq 180^\circ$. The effect of the inner diameter becomes to prevail with an increase in the gas flow rate.

(2) Porous nozzle

Bubble formation pattern depends on the diameter of a porous nozzle, as shown in Figs. 2.4, 2.5, and 2.6 [6]. Bubbles are successively generated from each hole of a wetted porous nozzle in the low gas flow rate regime. The bubble diameter, d_B , increases with an increase in the gas flow rate, Q_g . With a further increase in Q_g , some neighboring bubbles coalesce into a larger bubble in the course of rising in the bath (medium gas flow rate regime in Fig. 2.6). When the gas flow rate, Q_g , exceeds

Fig. 2.2 Bubble formation from wetted and poorly wetted nozzles in low gas flow rate regime

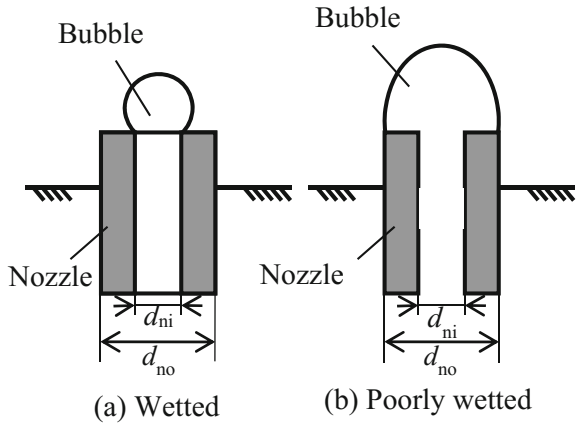
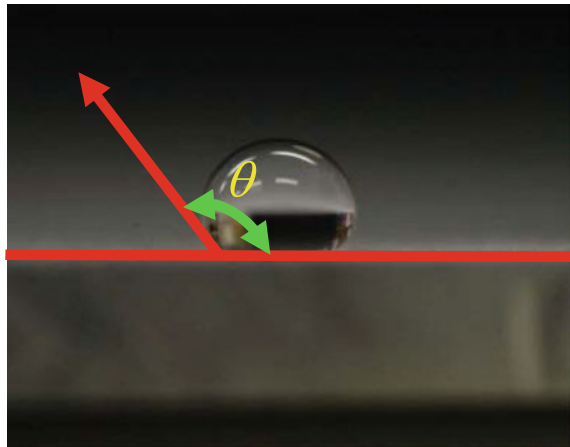
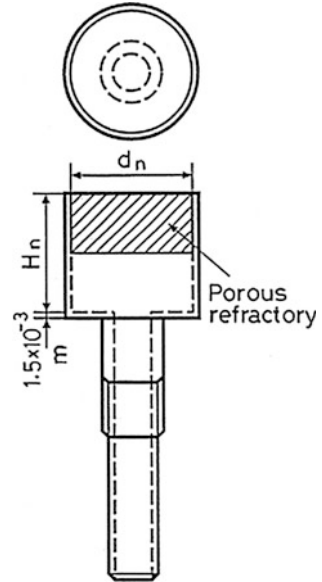


Fig. 2.3 Definition of equilibrium contact angle θ



a certain critical value, bubbles generated at the nozzle exit coalesce into a large single bubble just above the nozzle (high gas flow rate regime in Fig. 2.6). Meanwhile, in the case of a poorly wetted porous nozzle, the gas issuing out of each hole exit spreads along the surface of the nozzle and coalesce into a large single bubble regardless of the gas flow rate, although the evidence is not shown here. The nozzles employed in materials engineering at high temperatures are usually poorly wetted by molten metal, and hence, it is eventually difficult to generate small bubbles. Formation of small bubbles is desirable in this engineering field because metallurgical reactions are promoted with an increase in a total interfacial area between bubbles and molten metal.

Fig. 2.4 Shape and size of porous nozzle used in cold model experiment [6]



(3) Slot nozzle

A slot nozzle shown in Fig. 2.7 is one of the candidates for generating small bubbles in high-temperature materials processes [7]. Unfortunately, uniform bubble formation along the slot opening is not always realized, especially at high gas flow rates.

(4) Perforated plate

Gas is commonly introduced through a perforated plate into a wastewater pool for treatment in environmental engineering [8]. The plate has many holes, as schematically illustrated in Fig. 2.8. For example, air bubbles containing ozone are employed for wastewater treatment. The ratio of the hole diameter, d_h , to the plate thickness, L , (referred to as the diameter-to-length ratio) is nearly unity.

(5) Multi-hole nozzle

A multi-hole nozzle is a kind of perforated plates. The diameter-to-length ratio, d_{ni}/L , of the perforated plate is an order of the magnitude of unity, while the ratio of the multi-hole nozzle is usually much greater than unity [8].

(6) Perforated film

This film is suitable for generating fine bubbles [4]. The bubble diameter can be changed by controlling the pressure difference, $\Delta p (= p_{in} - p_{out})$. Here, p_{in} and p_{out} denote the inside and outside pressures, respectively.

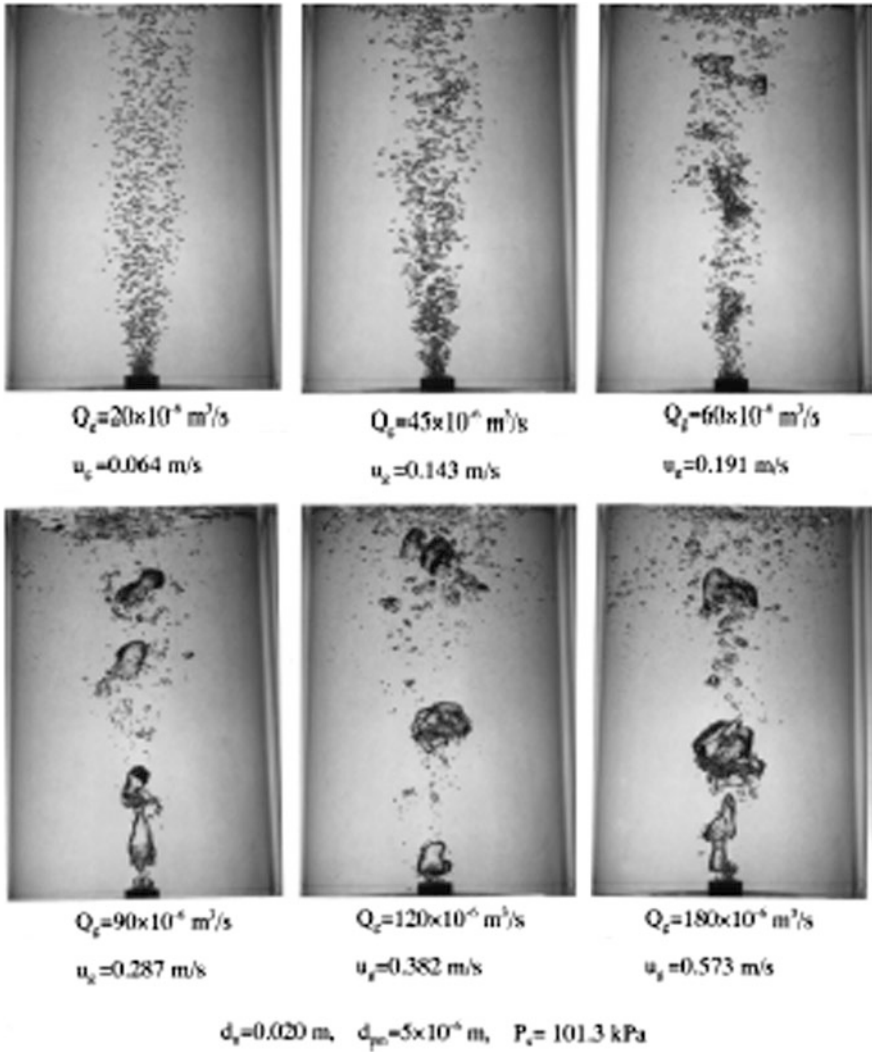


Fig. 2.5 Change in bubble dispersion patterns with volumetric gas flow rate (wetted porous nozzle, liquid: water, gas: air) [6]

(7) Speaker cone method

A speaker is connected to a single-hole nozzle to generate microbubbles [9, 10]. The diameter of the bubbles can be controlled by changing the frequency of pulse-like pressure fluctuation.

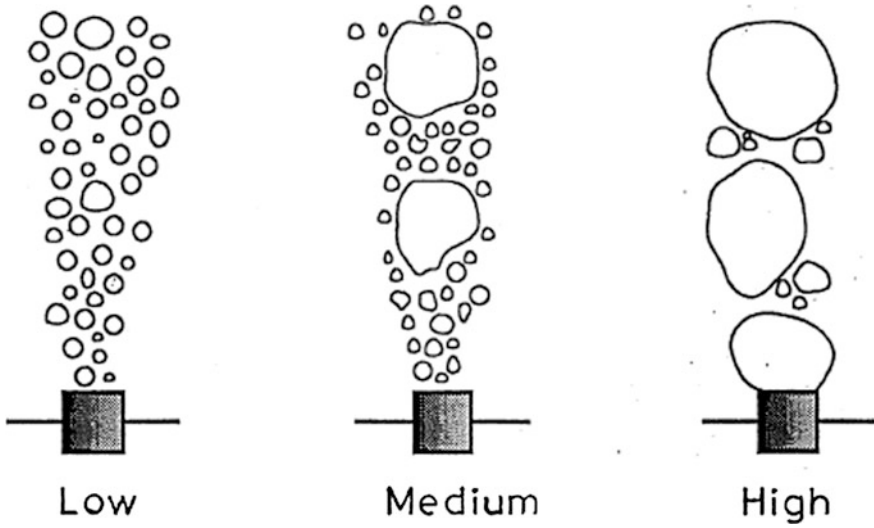


Fig. 2.6 Schematic illustration of dispersed bubbles in three gas flow rate regimes for a wetted porous nozzle [6]

Fig. 2.7 Bubble formation from a slot nozzle

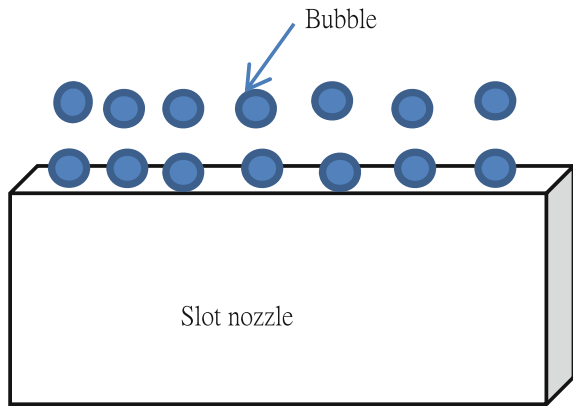
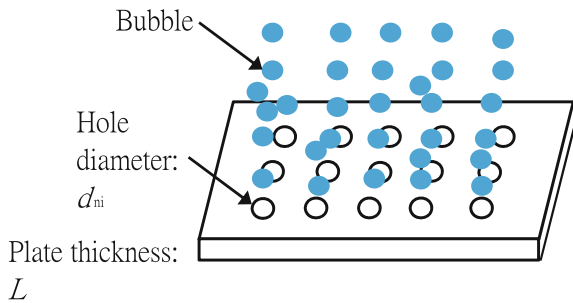


Fig. 2.8 Perforated nozzle commonly used in environmental engineering



(8) Shear stress imposition

The gas phase in a gas–liquid two-phase flow disintegrates into many smaller bubbles due to imposition of high shear stress [1, 11, 12]. As an example, disintegration of a bubble passing through a Venturi tube is schematically shown in Fig. 2.9.

(9) Cavitation method

A liquid changes into vapor bubbles when the liquid pressure is decreased below the vapor pressure of the liquid. This phenomenon is known as cavitation. Ultrasonic waves are imposed on a liquid to periodically cause cavitation. Bubbles appear and disappear alternatively under this condition [4].

(10) Pressurized dissolution method

The dissolution of gas into a liquid can be promoted by increasing the pressure of the liquid [4]. The gas thus dissolved becomes bubbles and escapes from the liquid with a decrease in the pressure. This phenomenon is successfully used for removing nonmetallic inclusions such as alumina (Al_2O_3) from molten iron in the steelmaking industry.

(11) Capillary wave method

When a bubble passes across the surface of a bath, the liquid film covering the front part of the bubble ruptures at a certain distance from the surface. Just after the rupture, the film shrinks in a wavy fashion so as to decrease its surface area as small as possible. This wave is called the capillary wave. The gas phase located near the crests of the wave in the bath disintegrates into many small bubbles [13].

(12) Plunging jet method

A liquid jet penetrating into a bath is referred to as a plunging jet. There appear four patterns depending on the surface roughness of the jet, as shown in Fig. 2.10 [14]. The plunging jet can be classified into three types: laminar, transitional, and turbulent jets. The jet type can be controlled by changing the liquid flow rate, Q_L , and nozzle height, h (distance from the nozzle exit to the bath surface). No bubble appears when the Reynolds number of the jet is very low in the laminar regime. This is because the surface of the jet is very smooth and, hence, any bubble cannot be captured at the bath surface. Here, the Reynolds number should be evaluated at the bath surface. With an increase in the jet Reynolds number, the surface of the jet becomes rough gradually and, as a result, many fine bubbles are generated. In the

Fig. 2.9 Disintegration of a bubble passing through a Venturi meter

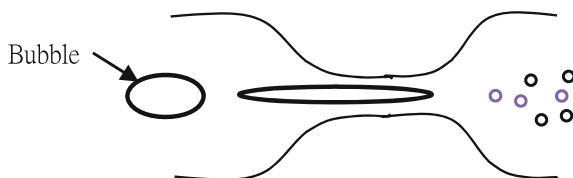
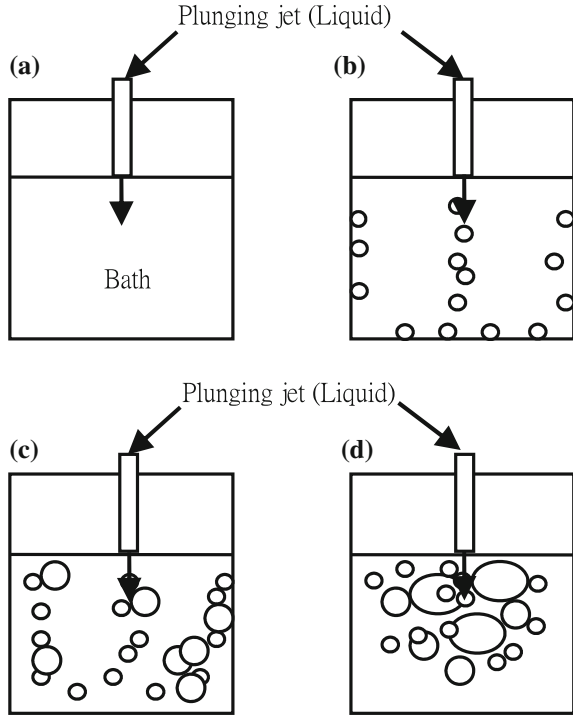


Fig. 2.10 Four-bubble entrapment patterns caused by a plunging jet (O: bubble). The plunging jet is **a** laminar at very low Reynolds number, **b** laminar, **c** transitional, and **d** turbulent



transitional regime, the surface becomes spontaneously rough. Such a rough surface triggers some large bubbles. Accordingly, a few large bubbles and many small bubbles coexist in the bath. The surface is very rough in the turbulent regime. Much more large bubbles are generated together with many small bubbles. The bubbles thus generated are removed from the bath surface due to the buoyant forces acting on them.

2.1.2 Generation Method of Droplet

The following methods originally proposed for bubble generation can be applied to droplet generation, as well [8]:

- (1) Single-hole nozzle,
- (2) Porous nozzle, and
- (3) Slot nozzle.

2.2 Experimental Setup

As a representative example, Fig. 2.11 shows a schematic diagram of an experimental apparatus for observing the three-dimensional structure of a bubbling jet. Water and air are chosen as models for molten metal and oxygen gas, respectively. Two sets of PIV systems are used, and the output images are processed on a personal computer to obtain velocity vectors in the bath. Detailed information on the image processing algorithm is given elsewhere [15].

2.2.1 Design of Nozzle and Its Mount for Visualization

In the steelmaking industry, injection conditions are basically classified into the following two types [16, 17]:

(1) Constant flow rate injection type

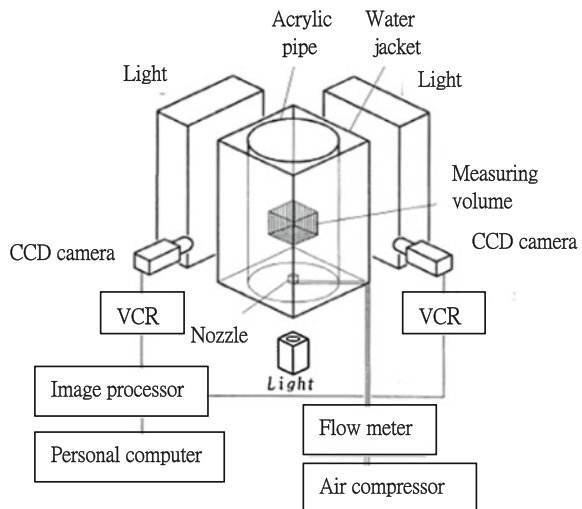
The pressure loss in a conduit between a gas supplying device (e.g., a compressor) and the nozzle exit is designed to be much greater than the pressure change during bubble formation. The flow rate of gas in the conduit can be kept constant regardless of the bubble formation.

(2) Constant pressure injection type

A large reservoir is placed just upstream of a nozzle, so that the pressure change during bubble formation is much smaller than the pressure at the nozzle inlet.

For the choice of the injection type, care must be taken not to induce the weeping of molten metal through the nozzle. In addition, information on the wettability of

Fig. 2.11 Schematic of experimental apparatus



the real nozzle is required for selecting nozzle materials in cold model experiments. As mentioned earlier, the bubble diameter depends strongly on the wettability of the nozzle.

2.2.2 Setup of Illumination for Visualization

Information on this subject also is referred to work by Uemura et al. [15].

2.3 Seeding Particle

The following two characteristics should be considered for the choice of seeding particles or tracer particles in particle tracking velocimetry (PTV) measurements:

- (1) Scattering characteristics of particles and
- (2) Tracking characteristics of particles.

Small diameters are required for adequate tracer response, while large diameters are necessary for a high signal-to-noise ratio of the scattered light signal. The diameter of tracer particles should be chosen by considering these two requirements.

Methods of generating seeding particles and introducing the particles into gas and liquid flows are explained in detail by Melling [18] and Matsumoto [19]. Tracer particles currently used in gas and liquid flows are listed in Tables 2.1 and 2.2, respectively.

Further information on tracer particles can be seen in Refs. [20, 21].

Table 2.1 Seeding particles in gas flows

Material	Density (kg/m ³)	Diameter (μm)	Remarks
TiO ₂	3500	<1	High temperature (<2500 °C)
Alumina (Al ₂ O ₃)	3970	<8	High temperature
Polycrystalline		30	
Glass	2600	30	
Olive oil	970	1.06	
SiO ₂	2200	1–5	
MgO	3650		Unstable
Silicone oil	≈900	1–3	Best
Glycerin	1261	0.1–5	Spray
Water	1000	1–2	Spray

Table 2.2 Seeding particles in liquid flows

Material	Density (kg/m ³)	Diameter (μm)	Remarks
TiO ₂	3500	3	
Al ₂ O ₃	3970	9.5	
Polymer	1000	30	
Reflective	1010	30, 60	
Fluorescent		20, 50	
Polystyrene	1050	15, 500	
Thermoplastic	1020	6	
Microsphere	700	<30	
Al powder	2380	<10	
Bubble	0.08	5–500	Hydrogen bubble
Glass beads	2600	10–150	
Latex	1030	0.5–90	Expensive
Milk	≈800	0.3=3	Cheap

2.4 Image Analysis

2.4.1 Introductory Remarks

The velocity of a fluid flow can be obtained by analyzing video images of small particles seeded in the fluid. This method is called particle image velocimetry (abbreviated as PIV), also referred to as particle tracking velocimetry (PTV). The techniques of PIV have advanced quickly because they have the following merits:

- (1) Instantaneous whole flow field measurement,
- (2) Contact-free measurement (noninvasive measurement), and
- (3) Easy extraction and processing of physical information through velocity information.

Some reviews on PIV [22–25] describe the principles and applications of many types of PIV, which are applicable from slow flows to supersonic flows.

The technical term “velocity” used in PIV means the velocity of particle motion, or the moving velocity of local small fluids elements with similar particle concentration distributions; on the assumption of good traceability of particle motion to fluid flow, the particle velocity can be taken as the fluid flow velocity. The size of the particles therefore must be so small that they can follow the fluid flow without relative velocity. This condition can be satisfied when the following particle Reynolds number, Re_p , is smaller than about unity:

$$Re_p = \frac{v_{pr} d_p}{\nu} < 1 \quad (2.3)$$

$$v_{pr} = v_f - v_p \quad (2.4)$$

where v_{pr} is the relative velocity (m/s), d_p is the particle diameter (m), ν is the kinematic viscosity of fluid (m²/s), v_f is the velocity of fluid (m/s), and v_p is the velocity of particle [m/s].

Whenever PIV is applied, the fluid flow is visualized by some tracer techniques. Visualization techniques, image recording materials, devices, and so on have been reported (e.g., [26]). In this section, we introduce some PIV techniques and propose a high-speed algorithm for two-dimensional (2D) and three-dimensional (3D) particle tracking velocimetry based on the binary cross-correlation method.

2.4.2 Classification of PIV

The techniques of PIV are classified, and their principles of velocity measurement are briefly introduced.

2.4.2.1 Multiple Exposure Techniques

- (1) **Pathline method:** The moving velocity of a particle is measured from the exposure time, photographing time, and particle image positions on a picture which is taken by a multiple exposure technique (Fig. 2.12). The velocity is determined by dividing the particle pathline length with the exposure time [27–29]. Using such a simple pathline technique, the start and end points of velocity vectors cannot be decided. In order to solve the problem of the flow direction, other techniques using vorticity information [30], brightness difference at the start and end points [31], color information [32], corded lighting at a short interval [33], independent photography of the start point and pathline [34], and so on are introduced.
- (2) **Stroboscope method:** When particle motions are photographed using a pulse-type lighting by a stroboscope, dotted lines of particle images are recorded on a picture. The velocity of the particle is measured from the distance between the dotted images and the lighting pulse interval. To get satisfactory measurement accuracy, the distance between dotted images should be longer than ten times the diameter of the particle image. This method can be applied to the flows of low particle number density but is not suitable for high particle number flows because of difficulty of particle identification.
- (3) **Laser speckle method:** When a fluid flow seeded with high-density small particles is illuminated by a pulse-type laser light sheet, random patterns of laser speckle are caused due to irregular interferences of scattered light from the particles [35, 36] (Figs. 2.13 and 2.14). After double or multiple recording of the speckle patterns on the same film at a short interval and calculation of autocorrelation of the patterns, particle velocities are obtained as the

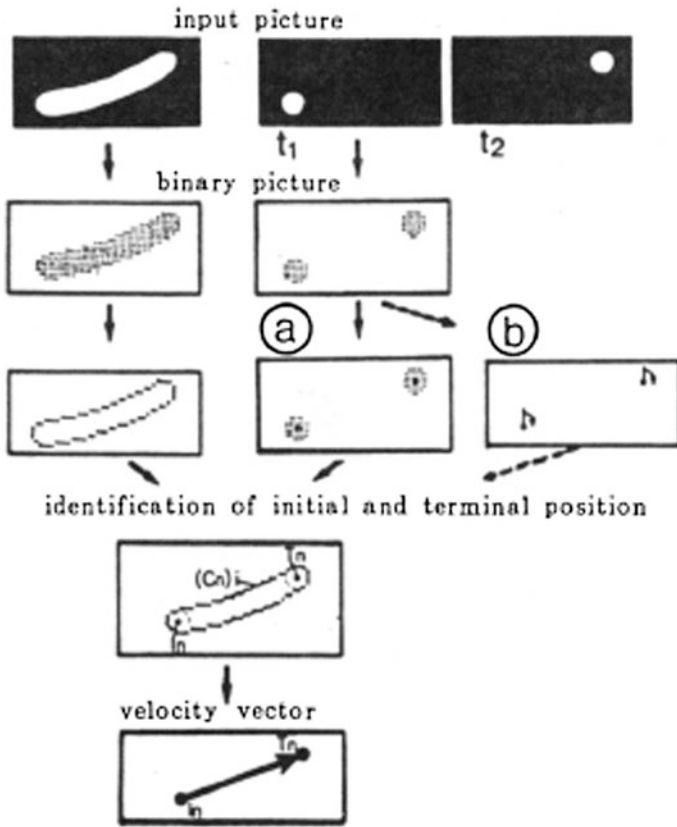
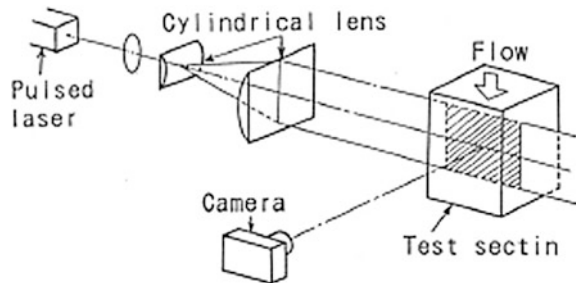


Fig. 2.12 Method of particle identification (independent photographing technique of start point, end point, and pathline)

Fig. 2.13 Lighting system and photograph system for speckle gram



information of pattern movements. A new dual-beam sweep illumination technique has been developed and applied to measure flow velocities in an aerosol jet [37]. The laser speckle method has a great merit for good traceability of small particle motion to fluid flows and is applicable to high-speed flows of about 100 m/s, unsteady turbulent boundary layer flows, and so on (Fig. 2.15).

Fig. 2.14 Young fringe optical system for local velocity measurement

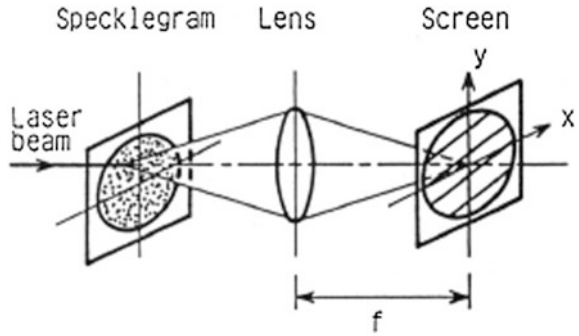
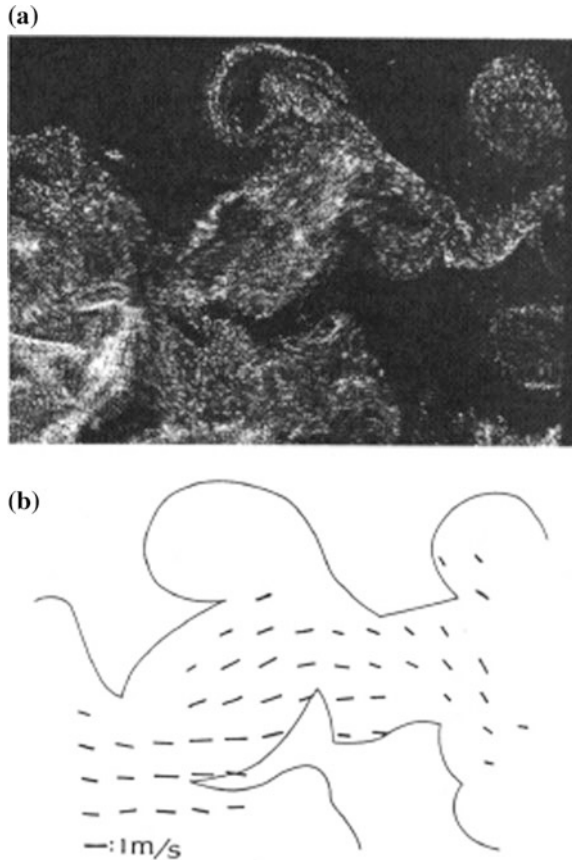


Fig. 2.15 Aerosol jet.
a Picture of a part of aerosol jet, **b** velocity vector diagram of aerosol jet by dual beam laser speckle technique



2.4.2.2 Method Using Consecutive Time-Step Patterns

- (1) **Four consecutive time-step particle tracking velocimetry (PTV):** Using consecutive four time-step pictures of flows visualized by particle tracers, which are photographed at a short interval, each particle is tracked and

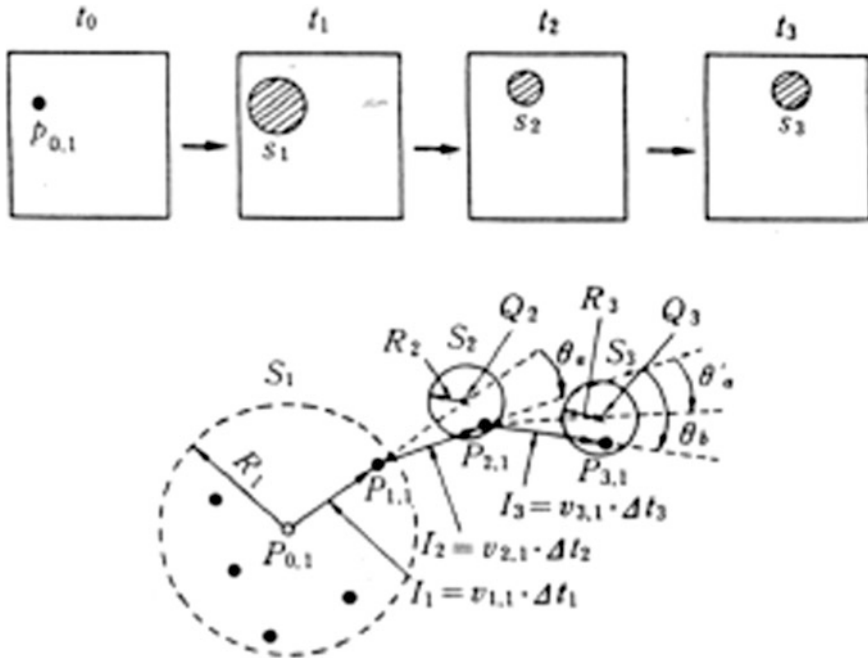
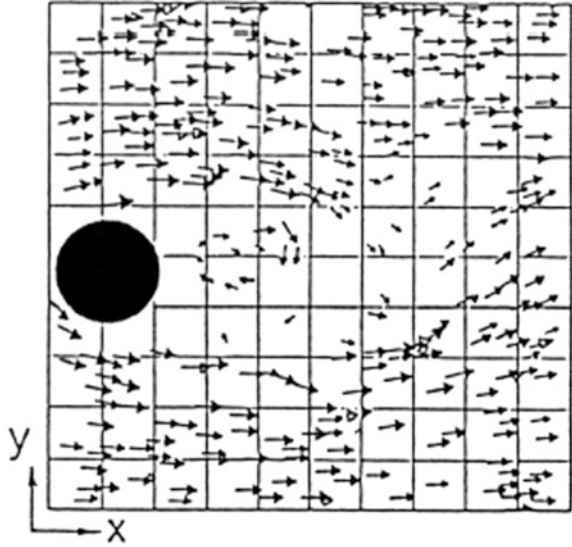


Fig. 2.16 Particle tracking using four consecutive particle tracking

identified (Fig. 2.16). The velocities of the particles are then calculated from the particle movement distances and the time interval. This method [31, 38–40] decides identification of each particle by investigating whether each trajectory of particle motion in the consecutive patterns is smooth or not (Fig. 2.17).

- (2) **Brightness (or concentration) distribution pattern cross-correlation method:** Tracking small local parts with the highest similarity of spatial brightness (concentration) distribution patterns in the two consecutive pictures visualized by small particles such as smoke of dyestuffs, velocities are calculated from the movement distances of the local parts and the time interval using cross-correlation method [41–43] (Fig. 2.18).
- (3) **Particle distribution pattern cross-correlation method:** This method, which has been developed by one of the authors [44, 45], tracks each particle motion in the two consecutive pictures, and its principle and applications are described in detail in the following section.

Fig. 2.17 Velocity vectors around a circular cylinder obtained by four consecutive time-step particle tracking technique



2.4.3 High-Speed Algorithm Based on Binary Cross-Correlation Method

2.4.3.1 Two-Dimensional Particle Tracking Velocimetry (2D PTV)

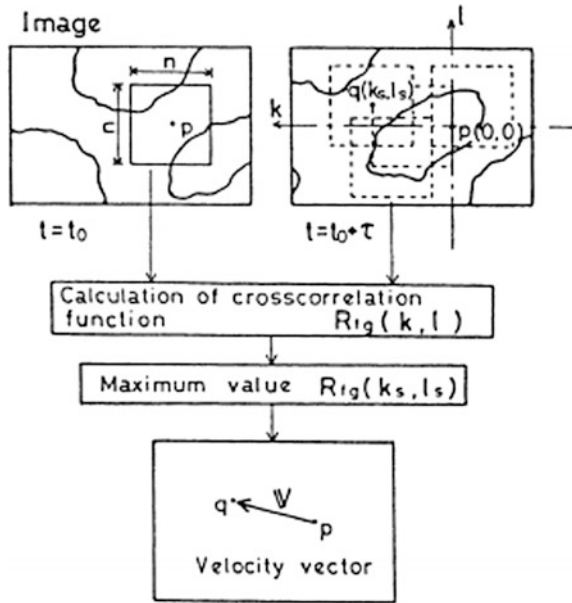
- (1) **Principle of particle identification:** Suppose that particle images in a 2D flow are captured at two times t and $t + \Delta t$ and that 2D coordinates of every particle center are calculated by some method, as shown in Fig. 2.19a and b.

The principle of particle identification in the two pictures is based on finding out a particle pair which has the best similarity in the particle distributions around a reference particle in the first picture and around a candidate particle in the second picture. In order to estimate the similarity in the two particle distribution patterns F and G , the following cross-correlation coefficient generally can be used:

$$C_{fg} = \frac{\sum_{i=0}^{n^2-1} (f_i - \bar{f})(g_i - \bar{g})}{\sqrt{\sum_{i=0}^{n^2-1} (f_i - \bar{f})^2 \sum_{i=0}^{n^2-1} (g_i - \bar{g})^2}} \quad (2.5)$$

where f and g are gray-level brightness values of pixels, which are elements of the materials F and G , at the center elements in which the reference particle image and the candidate particle images are located, respectively; f_i and g_i are brightness values of pixels of number i in the materials F and G , respectively. And \bar{f} and \bar{g} are

Fig. 2.18 Principle of cross-correlation method based on density distribution patterns



their mean values. However, if calculated strictly according to the definition in Eq. (2.5), the calculation takes considerably long time.

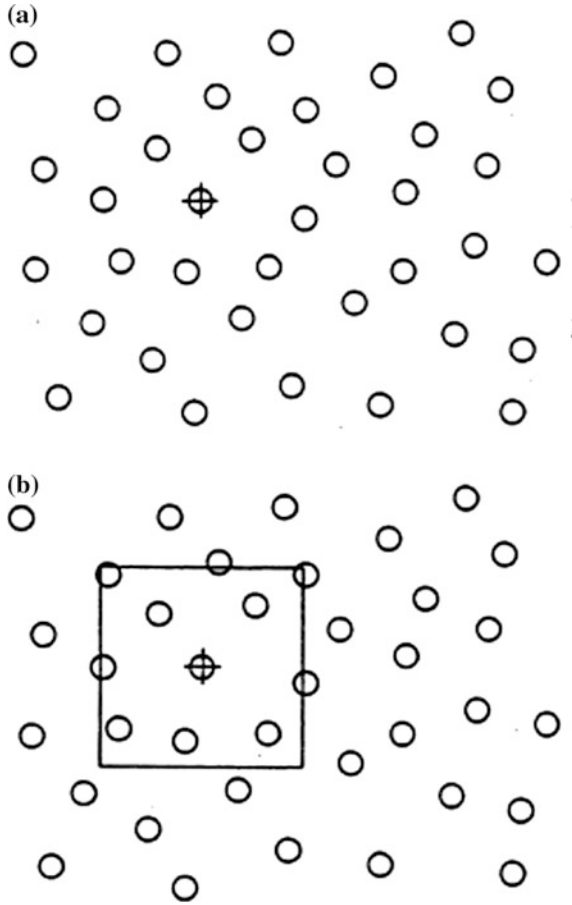
After the gray-level pictures with digital values of 0 to 255 are converted into binary pictures using an approximate threshold, f and g take the value of 1 inside the particle images and value of 0 outside of them. Now if two patterns I and J , with the same size at the centers of which a reference particle i and a candidate particle j are put, are overlapped at their center, the cross-correlation coefficient C_{ij} in such two binary pictures is expressed in the very simple form as follows:

$$C_{ij} = \frac{L}{\sqrt{mn}} \tag{2.6}$$

where m and n are the pixel number of particles in the reference pattern I of the first picture and in the candidate picture J of the second picture, and L is the summation of logical products of the two binary function f and g . In practice, L means the total area of overlapping parts of particle images in the overlapping two patterns, I and J , and the calculation of L can be done very quickly. Consequently, the value of C_{ij} can be computed in a very short time.

Figure 2.20 shows the flowchart of the binary cross-correlation method. Although several candidate particles are picked up to find out the particle identification for a reference particle, the candidate particle which gives the maximum value of C_{ij} is decided as the identified particle of the pair. The movement distance of the pair particle Δs is calculated as the distance between the two gravity centers, and the particle velocity is computed by the following equation:

Fig. 2.19 Images of particle distribution. **a** First picture, **b** second picture



$$\vec{v} = \frac{\Delta \vec{S}}{\Delta t} \quad (2.7)$$

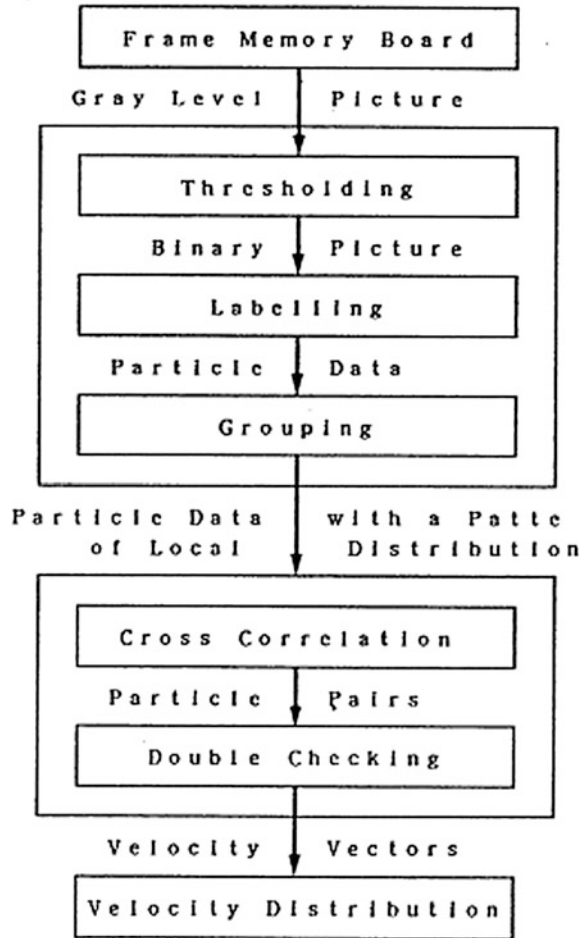
where Δt is the time interval between the two pictures.

Velocity vector distributions in a whole field are obtained from all the particle pairs corresponded by the above algorithm. Figure 2.21 shows an example of the image processing system of 2D PTV which is used here.

(2) Application of 2D PTV

After the 2D unsteady viscous diffusing doublet flow is visualized by the hydrogen bubble technique and 2D PTV is applied, the velocity vectors are obtained as shown in Fig. 2.22. As shown in this figure, the fluid is engulfed upstream of the doublet and squeezed out downstream of the doublet. Computation of $\text{rot } \vec{v}$ presents the vorticity contours as shown in Fig. 2.23a and b. From comparison of these

Fig. 2.20 Flowchart of binary picture cross-correlation method



figures, it is shown that the positions of the vorticity peaks flow downstream with the lapse of time and the vorticity is diffusing.

Figure 2.24 shows the water flow field in the suddenly expanding part of a channel after flow visualization by plastic particle tracers. This is a flow field consisting of the slow flow in the reverse flow region after the suddenly expanding part and the fast parallel flow in the upper part. In this case, flexible size of correlation spaces for particle identification is essential.

Figure 2.25 represents the velocity vectors of particles which are randomly scattered and fixed on a rotating disk. Such an experiment is useful for the calibration test of 2D PTV because every particle velocity is known from the rotating speed of the disk and the radius position of each particle. Comparing the known data with experimental results, the mismatched correspondence of particle pairs and measurement accuracy can be investigated. Actually, some particle pairs which result from mismatched correspondence cannot be avoided by the correlation

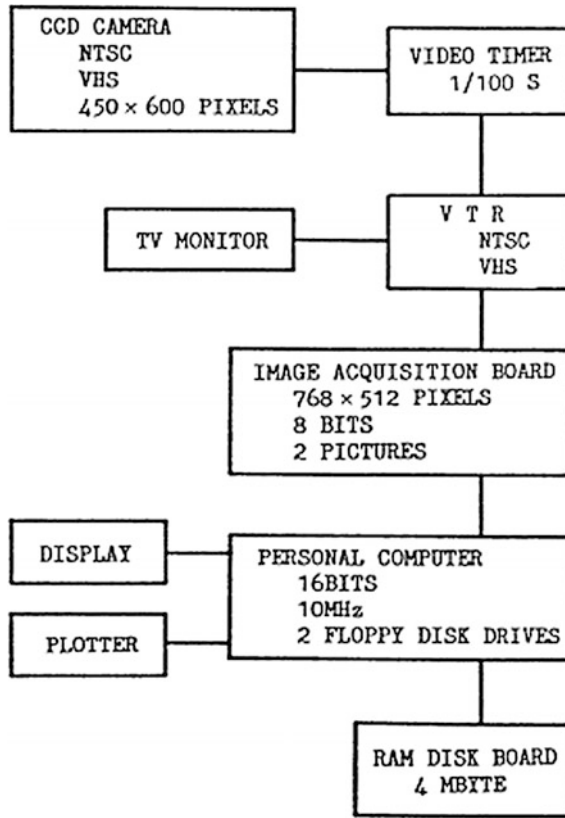


Fig. 2.21 Image processing system

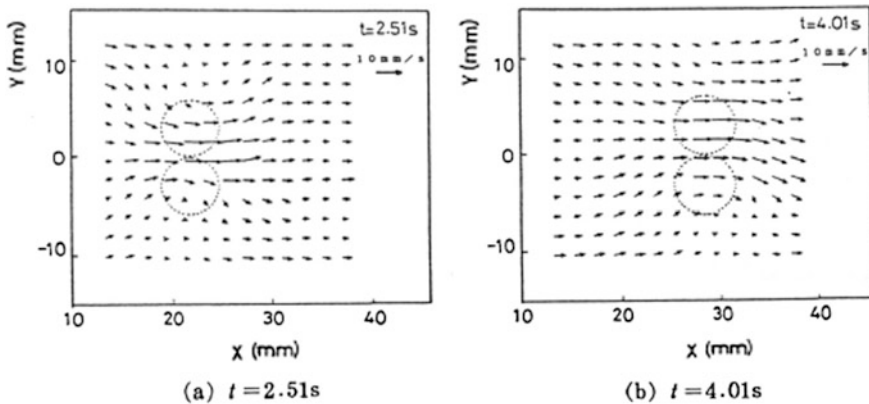


Fig. 2.22 Velocity vectors of a viscous diffusing doublet flow

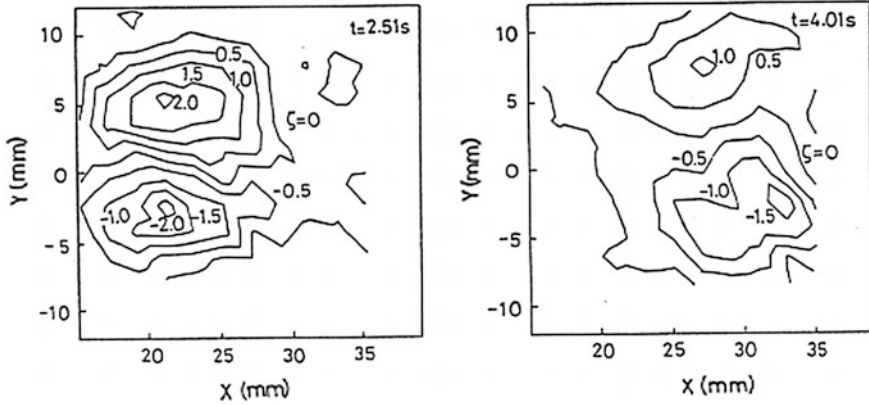
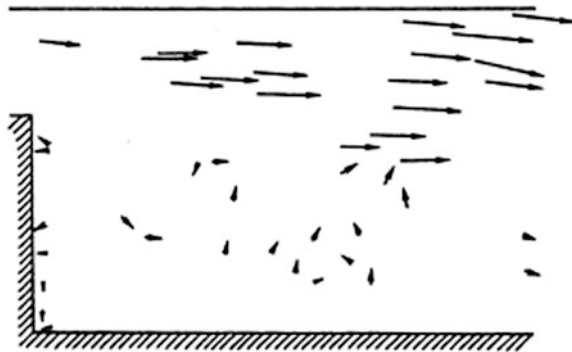


Fig. 2.23 Vorticity contours of a viscous diffusing doublet flow

Fig. 2.24 Velocity vectors of flow in suddenly expanding channel

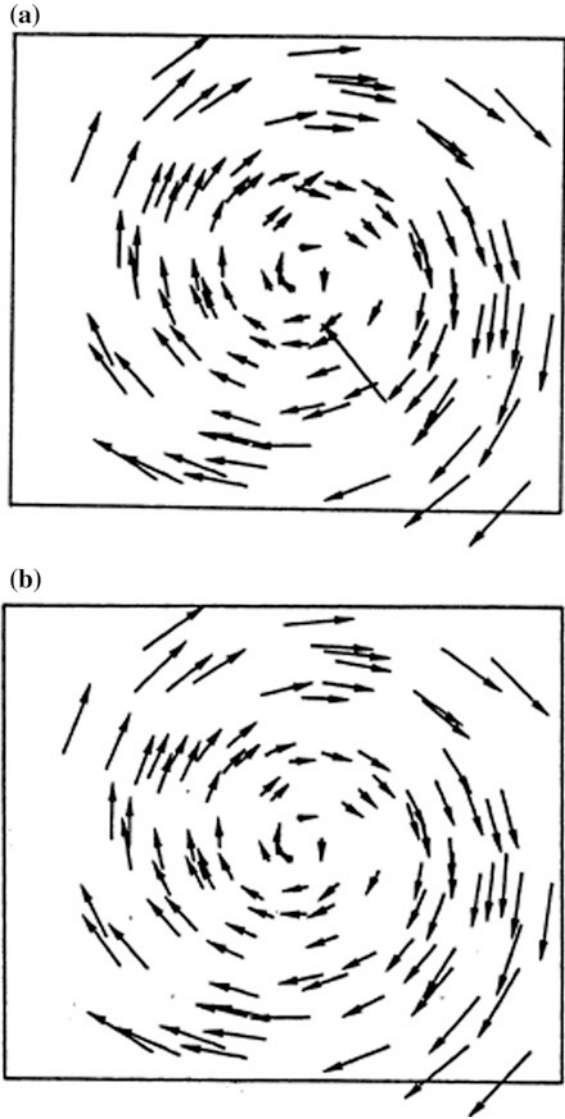


method. It is proposed a so-called double checking method, which uses the second and the third maximum values of C_{ij} and estimates the reliability of the correct matching of particle pairs [45]. Figure 2.25a contains some mismatched velocities before the application of double checking, but Fig. 2.25b shows all correct velocity vectors after the mismatched velocity vectors have been replaced by the correct ones.

Figure 2.26 shows the velocity vectors of a sink flow in a water reservoir after flow visualization by plastic particle tracers. Figure 2.26a shows the results before the double checking, and some mismatched velocity vectors are seen in it. The reason of the mismatched correspondence is that some particles flow at a higher speed and connect each other near the sink port. Such mismatched velocity vectors are replaced with the correct ones by the double checking as shown in Fig. 2.26b.

Figure 2.27 shows an example of velocity measurement of a flow behind a moving sphere. Since a sphere is a 3D shape, the resultant velocity vectors are the projected components of 3D velocities on a 2D light sheet with a finite thickness. As shown in Fig. 2.28, a particle which crosses the light sheet at a time interval dt at a very high speed, and particles which come in it or go out from it, cannot be

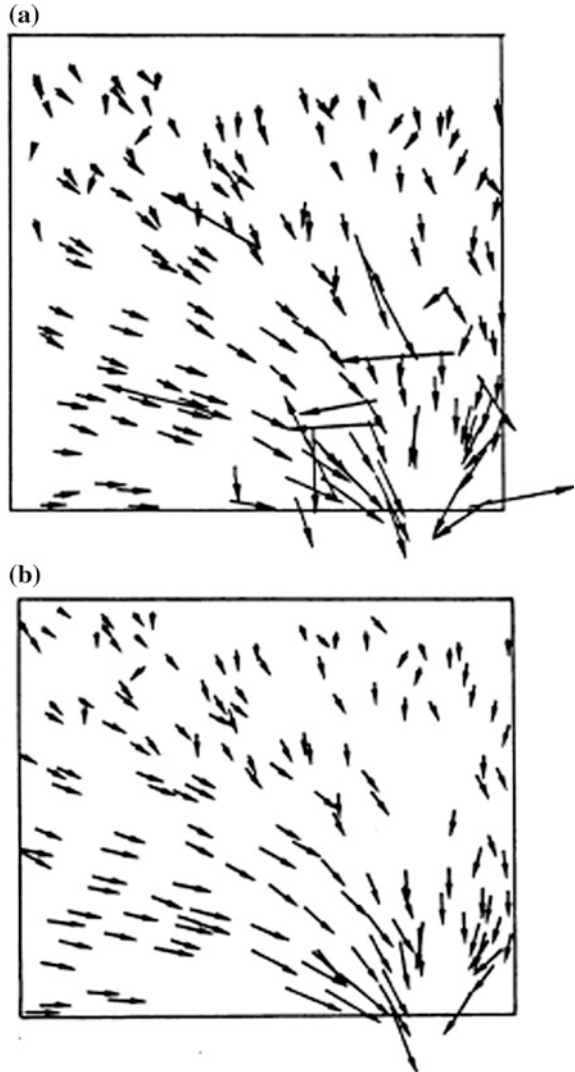
Fig. 2.25 Particle velocities on a rotating disk. **a** Before double checking, **b** after double checking



tracked. Such particles are excluded from the object of the measurement. Therefore, the number of resultant velocity vectors is smaller than the real particle number in the light sheet, and if the average velocity in a part of such a 3D flow is computed, it may be slower than the real velocity.

Figure 2.29 shows a visualized picture of mixing flows with a bubbling jet in a cylindrical bath. The tracers are plastic particles with diameter of 0.8 mm. After capturing such fifty-one picture frames and analyzing the images between consecutive two frames repeatedly, velocity vectors were obtained. Figure 2.30 is one

Fig. 2.26 Velocity vectors in a sink flow. **a** Before double checking, **b** after double checking



of them. Figure 2.30a shows the instantaneous velocities at the particle positions, and Fig. 2.30b shows the rearranged velocities at grid points. In both the figures, big circulation flows are seen in the upper part of the bath and zigzag upward flows are seen along the centerline of the bath. Figure 2.31 represents the time mean velocity vectors computed from the fifty charts of instantaneous velocity vectors. In this figure, the zigzag flows cannot be seen. Figure 2.32 shows distributions of the RMS values of velocity fluctuations in the cylindrical bath. The RMS values are big at the upper part of the bath because there exist strong circulation flows. It is noted that the above-mentioned fluctuation flows and zigzag flows promote the mixing of water in the bath by the bottom-blowing bubbling jet.

Fig. 2.27 Velocity vectors of flow after a moving sphere

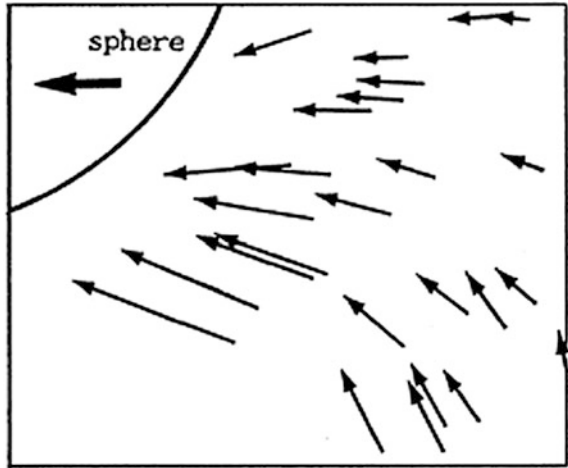
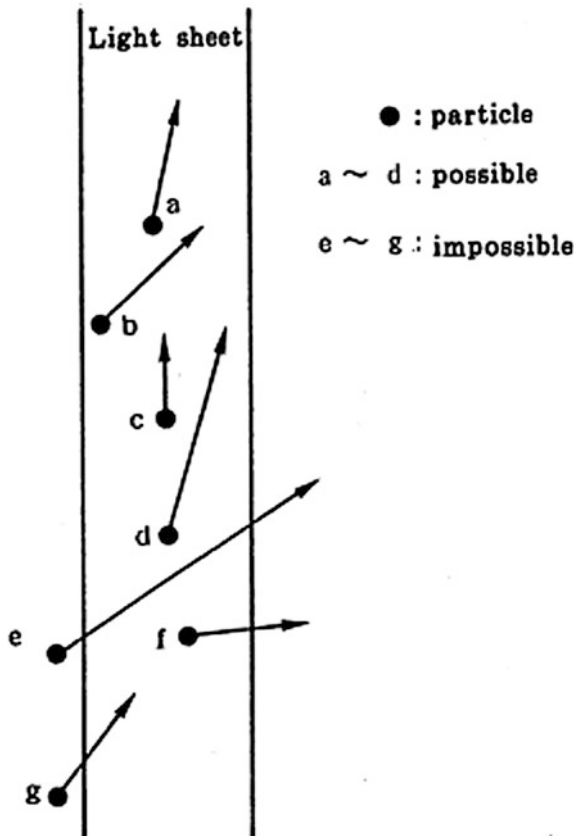


Fig. 2.28 Particle motions in a light sheet



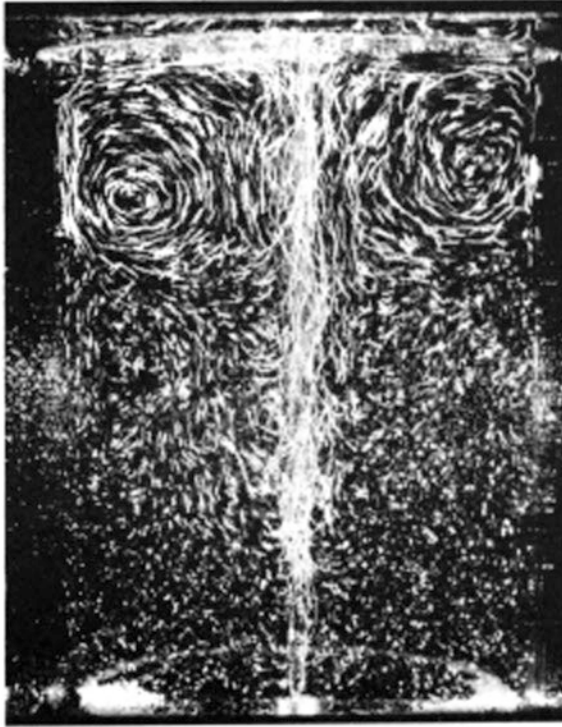


Fig. 2.29 Mixing flow with air bubbling jet in a cylindrical bath

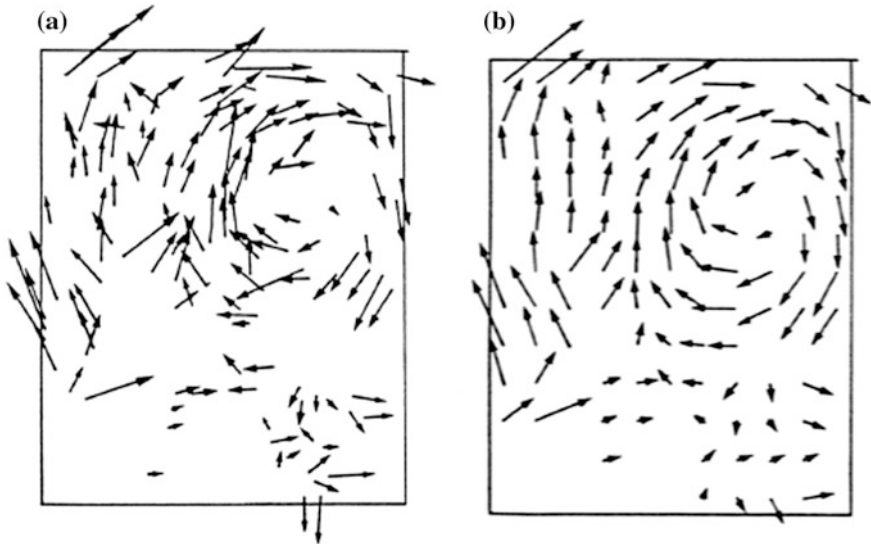


Fig. 2.30 Instantaneous velocity vectors of the mixing flows. **a** At particle positions, **b** rearranged at grid points

2.4.3.2 Three-Dimensional Particle Tracking Velocimetry (3D PTV)

- (1) **Principle of particle identification:** Here, we assume that 3D coordinates of every particle center in flow fields are already calculated from two or three picture frames of particle images taken simultaneously and that the two groups of coordinates of particle images at time t and $t + \Delta t$ are known. The present problem is how to find particle pairs in the first space at time t and the second space at $t + \Delta t$. The answer is based on the following 3D binary correlation method.

The practical space and size of each particle are unfixed in the digital image pictures. If they are changed into approximate uniform space and size, the performance of the image analysis can be improved. Such particles are called imaginary particles, whose coordinates of gravity centers are kept the same as those of the practical images. Using the principle of the particle distribution similarity to find out particle pairs in two 3D spaces, the following cross-correlation coefficient defined for two patterns as follows might be adopted:

$$C_{fg} = \frac{\int f(x, y, z) \cdot g(x, y, z) dV}{\sqrt{\int \{f(x, y, z)\}^2 dV \int \{g(x, y, z)\}^2 dV}} \quad (2.8)$$

Unfortunately, the calculation of the value of C_{fg} according to the definition will take a very long time. If imaginary particles in the binary pictures are employed, the cross-correlation coefficient C_{fg} for the two particle distribution patterns I and J is expressed in the following simple form:

$$C_{ij} = \frac{f(\overline{Sk})}{\sqrt{N_i N_j}} \quad (2.9)$$

where $\overline{Sk} = Sk/d$ is the normalized distance between gravity centers of any overlapped particle pairs after overlapping the two patterns I and J , N is the number of the overlapped particle pairs, d is the diameter or characteristic length of the imaginary particle, and N_i and N_j are the numbers of particles in the patterns I and J, respectively [46]. The function $f(\overline{Sk})$ represents the ratio of overlapped volume of any overlapped particle pair k to the volume of imaginary particle. When two particles of a pair are completely overlapped, $f(\overline{Sk}) = 1$, and when two particles are separate from each other, $f(\overline{Sk}) = 0$. The function $f(\overline{Sk})$ is given for spherical shape of imaginary particle by the following equation:

$$f(\overline{Sk}) = 1 - \frac{3}{2}\overline{Sk} + \frac{1}{2}\overline{Sk}^3 \quad (2.10)$$

If the value of C_{ij} takes the maximum value for a pair of a reference particle and a candidate particle, the candidate particle is decided as the identified particle of the reference particle.

(2) Simulation results

To investigate the particle identification performance of the 3D PTV, numerical simulation experiments were carried out using a 3D unsteady viscous doublet flow, which is expressed as an analytical solution of 3D Oseen's equation [47]. Although an example of the 3D velocity vectors of the doublet flow is not shown here, comparison of the velocities by the analytical solution and the simulation results made clear that almost all of the 126 particles were identified and the velocities were measured correctly.

2.4.4 Concluding Remarks

A high-speed algorithm of 2D and 3D particle tracking velocimetry based on the binary picture cross-correlation method was proposed, and some measurement results were presented [48]. The technique may be said to be useful for practical applications.

Further information on PIV should be referred to Refs. [49–52].

References

1. K. Mori, M. Sano, Process kinetics in injection metallurgy. *Tetsu-to-Hagane* **67**, 672 (1981)
2. K. Mori, M. Sano, Y. Ozawa, Recent studies in process science of injection metallurgy. *Tetsu-to-Hagane* **69**, 1714 (1983)
3. M. Takahashi et al., *Recent Technologies on Fine Bubbles* (NTS, Tokyo, 2006)
4. CMC, *Applications of Micro and Nano bubbles to Environmental Engineering* (CMC, Tokyo, 2006)
5. S.E. Gaddis, A. Vogelpohl, *Chem. Eng. Sci.* **41-1**, 97–105 (1986)
6. M. Iguchi, M. Kaji, Z. Morita, *Metall. Mater. Trans. B* **29**, 1209–1218 (1998)
7. K. Okumura, S.V. Komarov, M. Sano, Gas injection from slot nozzles with various shapes in water. *ISIJ Int.* **40-6**, 544–548 (2000)
8. Soc. Chem. Eng. Jpn., *Handbook of Chemical Engineering* (Maruzen, Tokyo, 1999), p. 481
9. A. Kariyasaki, A. Ousaka, in *Proceedings of 5th International Conference on Gas-Liquid and Gas-Liquid-Solid Reactor Engineering* (2001), pp. 460–468
10. T. Sanada, M. Watanabe, T. Fukano, A. Kariyasaki, *Chem. Eng. Sci.* **60**, 4886–4900 (2006)
11. Yamamura, R. Kamijima, M. Mizukami, K. Amata, K. Miawa, K. Takase, *Curr. Adv. Mater. Process.* **10-1**, 137 (1997)
12. K. Okumura, S.V. Komarov, M. Sano, *ISIJ Int.* **40-6**, 544–548 (2000)
13. T. Uchida, M. Iguchi, *J. Mater. Process. Manuf. Sci.* **8-1**, 256–264 (2000)
14. M. Iguchi, K. Okita, F. Yamamoto, *Int. J. Multiphase Flow* **24-4**, 523–537 (1998)
15. T. Uemura, F. Yamamoto, M. Iguchi, Z. Morita, T. Usui, J. Ohta, in *Proceedings of 1st Visualization and Intelligent Design in Engineering and Architecture*, Southampton (1993), pp. 389–403
16. K. Mori, M. Sano, Process kinetics in injection metallurgy. *Tetsu-to-Hagane* **67**, 672 (1981)
17. M. Iguchi, *Tetsu-to-Hagane* **103**, 119 (2017)

18. A. Melling, Tracer particles and seeding for particle image velocimetry. *Meas. Sci. Technol.* **8**, 1406–1416 (1997)
19. M. Matsumoto, The Visualization Society of Japan (eds.), *Committee for Standardization of PIV, Lecture Course Textbook* (1993)
20. M. Yano, S. Umeda, K. Dan, Motion of tracer particle. *Flow Vis.* **6-22**, 131–136 (1986)
21. M. Muraoka, T. Kumagai, On the motion of a tracer particle in unsteady flows. *Trans. JSME B* **59-559**, 713–720 (1993)
22. L. Hesselink, Digital image processing in flow visualization. *Ann. Rev. Fluid Mech.* **20**, 421–485 (1988)
23. JSME, JSME Lecture Course Textbook for Freshmen, Capture Flows, JSME Textbook No. 910-40 (1991)
24. R.J. Adrian, Particle-imaging techniques for experimental fluid mechanics. *Ann. Rev. Fluid Mech.* **23**, 261–304 (1991)
25. The Visualization Society of Japan (eds.), Correlation-velocity measurement using image correlation, in *3rd Lecture Course Textbook* (1991)
26. The Visualization Society of Japan (eds.), *New Handbook Flow Visualization* (Asakura-Shoten, Tokyo, 1986)
27. K. Imaichi, K. Ohmi, Numerical processing of flow-visualization pictures-measurement of two-dimensional vortex flow. *J. Fluid Mech.* **129**, 283–311 (1983)
28. M. Takagi, T. Tomita, Measurement processing of flow visualization, in *Proceedings of the 11th Images Processing Conference*, vol. 9 (1984), pp. 12–16
29. T. Kobayashi, Y. Yoshitake, Development of digital image processing system for pathline pictures. *Trans. JSME (B)* **51-466**, 1966–1970 (1985)
30. P.E. Dimotakis, F.D. Debussy, M.M. Koochesfahani, Particle streak velocity field measurements in a two-dimensional mixing layer. *Phys. Fluids* **24-6**, 995–999 (1981)
31. T. Kobayashi, T. Saga, S. Segawa, H. Kanda, Development of a real-time velocity measurement system for two-dimensional flow fields using a digital image processing technique. *Trans. JSME (B)* **55-509**, 107–115 (1989)
32. T. Fjiwara, S. Nishihara, K. Hirose, Color flow-visualization photography and digital image processing techniques. *Trans. JSME (B)* **53-493**, 2762–2770 (1987)
33. B. Khalighi, Study of the intake swirl process in an engine using flow visualization and particle tracking velocimetry. *AME-FED* **85**, 37–47 (1989)
34. T. Kobayashi, Development of a flow field analysis system using a digital image processing technique, Report of Grant 1986-C for Scientific Research by the Japan Ministry of Education (1988)
35. M. Kawahashi, Laser speckle method. *J. Vis. Soc. Jpn.* **7-25**, 84–89 (1987)
36. M. Kawahashi, Speckle method, in *3rd Lecture Course Textbook* (1991), pp. 58–60
37. M. Kawahashi, K. Hosoi, *Exp. Fluids* **11**, 278–280 (1991)
38. N. Tsuda, T. Kobayashi, T. Saga, Development of a real-time velocity measurement system for high Reynolds number fluid flow using a digital image processing technique. *J. Vis. Soc. Jpn.* **11**(Suppl. No. 1), 181–184 (1991)
39. T. Kobayashi, T. Saga, T. Haeno, N. Tsuda, Development of a real-time velocity measurement system for high Reynolds number fluid flow using a digital image processing design. *ASME-FED* **128**, 9–14 (1991)
40. N. Tsuda, T. Kobayashi, T. Saga, Development of a general use PIV system, in *Proceedings of 6th Osaka Symposium on Flow Measurement* (1991), pp. 47–52
41. I. Kimura, H. Kimura, T. Takamori, Image processing of flow around a circular cylinder by using correlation technique, in *Proceedings of 4th International Symposium on Flow Visualization* (Hemisphere Pub. Corp., 1986), pp. 221–226
42. J. Sakakibara, T. Takada, K. Kobayashi, K. Hishida, M. Maeda, Two dimensional and time series measurement of thermally stratified shear flow by using correlation technique. *J. Vis. Soc. Jpn.* **11-1**, 157–160(1991)
43. T. Kobayashi, J. Sakakibara, K. Hishida, M. Maeda, Time-series measurement of turbulent flow field using image processing system. *ASME-FED* **128**, 55–162 (1991)

44. F. Yamamoto, T. Uemura, M. Koukawa, M. Itoh, A. Teranishi, Application of flow visualization and digital image processing techniques to unsteady viscous diffusing free doublet flow (in the case of impulsive concentrated drag application), in *Proceedings of 2nd FLUCOME* (1988), pp. 184–188
45. T. Uemura, F. Yamamoto, M. Koukawa, High-speed algorithm for particle tracking velocimetry-using binary. *J. Vis. Soc. Jpn.* **10-38**, 196–202 (1990)
46. F. Yamamoto, T. Uemura, M. Iguchi, High speed algorithm of 2D and 3D PTV based on binary correlation method, in *Proceedings of 1992 International Seminar on Imaging in Transport Processes*, Athens (1992), pp. 321–332
47. S. Murata, Y. Miyake, Y. Tsujimoto, F. Yamamoto, Study of three-dimensional unsteady Oseen flow. *J. Fluid Mech.* **86-4**, 609–622 (1978)
48. Y. Fujio, T. Uemura, Fundamentals and applications of PIV. *Jpn. J. Multiphase Flow* **6-1**, 65–79 (1992)
49. W.-J. Yang, *Handbook of Flow Visualization*, 2nd edn. (Taylor & Francis, New-York, 2001)
50. I. Kimura, T. Uemura, T. Okuno, *Visualized Information Measurement* (Kindaikagaku Co. Ltd., Tokyo, 2001)
51. The Visualization Society of Japan (eds.), *Handbook of Particle Image Velocimetry* (Morikita Shuppan Co. Ltd., Tokyo, 2002)
52. A. Schroeder, C.E. Wille, *Particle Image Velocimetry-New Developments and Recent Applications* (Springer, Berlin, 2007)



<http://www.springer.com/978-4-431-56565-9>

Flow Visualization in Materials Processing
Practical Techniques and Selected Applications

Uemura, T.; Ueda, Y.; Iguchi, M.

2018, XIII, 218 p. 194 illus., 48 illus. in color., Hardcover

ISBN: 978-4-431-56565-9